

## Exploring Nanoparticle Porosity Using Nano-Impacts: Platinum Nanoparticle Aggregates<sup>†</sup>

Received 00th January 20xx,  
Accepted 00th January 20xx

Xue Jiao,<sup>a</sup> Stanislav V. Sokolov,<sup>a</sup> Eden E. L. Tanner,<sup>a</sup> Neil P. Young<sup>b</sup> and Richard G. Compton,<sup>\*a</sup>

DOI: 10.1039/x0xx00000x

www.rsc.org/pccp

**The porosity of platinum nanoparticles (PtNPs) is explored for the first time using tag-redox coulometry (TRC). This is achieved by monitoring the reduction of the 4-Nitrobenzenethiol(NTP)-tagged PtNPs on carbon electrodes via both immobilisation and nanoimpacts. The average charge per impact is measured and attributed to the reduction of NTP adsorbed on individual PtNPs. The number of NTP molecules and thus the “active surface area” of the PtNPs is calculated and compared with two models: fully solid and porous nanoparticles, and the extent of the particle porosity revealed. This allows a fuller understanding of the (electro)-catalytic behaviour of nanoparticles by providing insight into their porosity and “true/active surface areas”.**

Nanoparticles find ever increasingly diverse applications embracing the catalysis of chemical and biochemical reactions, the electrocatalysis of electrode reactions, especially those important for energy transformation processes and environmental remediation.<sup>1–7</sup> Key to many uses, both fundamental and applied, is the availability of very high surface areas, in relation to mass, in comparison with conventional materials. This can significantly promote the adsorption of molecular species which often lies at heart of the physical and chemical process of interest. Whilst this is encouraged by the intrinsic nanoscale of the particles it can be further enhanced if the nanoparticles themselves show significant nanoporosity. This can be realised synthetically by the aggregation during formation of ultra-small nanoparticles clumping together to form porous larger nanoparticles<sup>8</sup> or by the initial formation of alloys followed by a dealloying protocol which selectively removes one of the alloy components.<sup>9</sup> Nanoporosity has been suggested variously to lead to improved adsorption in environmental applications,<sup>10–14</sup> catalysed oxygen reduction kinetics,<sup>15–18</sup> changed optical properties<sup>19–20</sup> and enhanced pseudocapacitor performance.<sup>21</sup>

Many of the applications of porous nanoparticles involve their being exposed to a solution phase where they might form a coating on an electrode, adsorb environmental targets or catalyse a desired reaction. It is therefore of interest to develop experiments to probe the extent to which the internal surfaces of a porous nanoparticle ‘see’ the surrounding solution phase, or to put the issue in a different form, to find the extent to which the internal surfaces of a porous nanoparticle or nanoparticle aggregate are accessible to solution phase species. Traditionally such nanoporosity has been accessed via *ex situ* gas phase adsorption isotherm approaches, such as the Brunauer-Emmett-Teller (BET) method. However the qualitative contrast between gas/solid and liquid/solid interfaces coupled with the very small size of the molecules (such as nitrogen) used in gas adsorption measurements makes the development of *in situ* approaches desirable.

In this paper we report on the use of the nanoimpacts method to measure the surface coverage of redox active molecules adsorbed on the surface of platinum nanoparticles (PtNPs) (ca. 50 nm diameter) which are themselves composed of aggregates of much smaller particles and for which transmission electron microscopy (TEM) reveals significant nanoporosity. In the nanoimpacts method<sup>22–25</sup> single nanoparticles suspended in solution from time to time impact on the surface of a microelectrode by virtue of their Brownian motion. If the electrode is held at a suitable potential the nanoparticle itself may be oxidised or reduced<sup>26–27</sup> or, in the case of the experiments reported below, surface layers of adsorbate on the particles may be electrolysed. Measurement of the charge then, in the latter case, shows the extent of the surface coverage which, when compared with TEM data, allows an assessment of the particle porosity and the scale to which the internal surfaces of the porous particles are accessible to the solution phase.

The PtNPs used were found to be made up of an aggregation of smaller particles (around 2.5 nm radius from TEM), and typical images are shown in Fig. 1(a) and (b). A total of 165 PtNP aggregates were sized and their radii calculated, as

<sup>a</sup> Department of Chemistry, Physical and Theoretical Chemistry Laboratory, University of Oxford, South Parks Road, Oxford OX1 3QZ, United Kingdom.

<sup>b</sup> Department of Materials, University of Oxford, Parks Road, Oxford OX1 3PH, United Kingdom.

<sup>†</sup> Electronic Supplementary Information (ESI) available. See DOI: 10.1039/x0xx000x

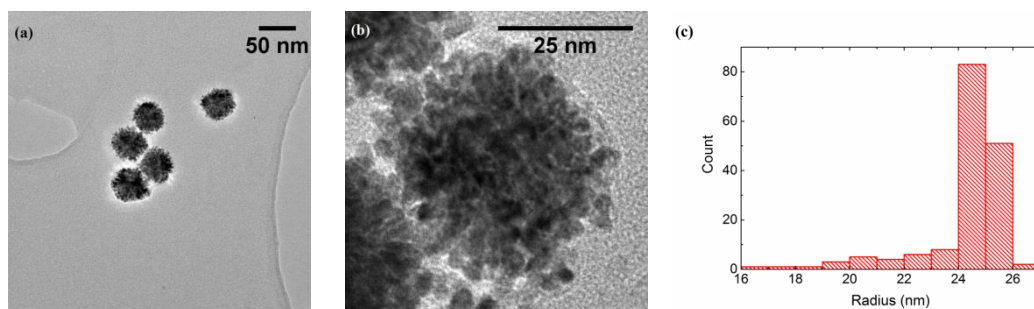
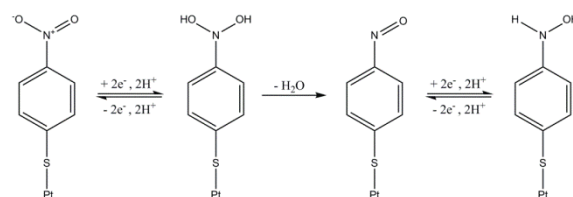


**Fig. 1** (a) TEM bright field image of PtNPs. (b) High-resolution TEM image of one PtNP. (c) Size distribution of the PtNPs with an average radius of  $24.3 \pm 1.6$  nm.

shown in Fig. 1(c). A mean radius of  $24.3 \pm 1.6$  nm was obtained, close to the value of 25 nm provided by the manufacturer. To clarify, in this paper, "PtNP" refers to the platinum nanoparticle aggregate (ca. 25 nm radius), and "small nanoparticle" is the component of a PtNP (ca. 2.5 nm radius).

The porosity of PtNPs was next established by tag-redox coulometry (TRC). This was achieved through the electrochemical analysis of 4-Nitrobenzenethiol (NTP) reduction using both cyclic voltammetric and nanoimpact techniques. First, a glassy carbon macroelectrode was modified either by immersion into an NTP solution or drop casting a NTP-tagged PtNP suspension and recording cyclic voltammograms (CVs). Second, an overpotential was carefully selected from voltammetric measurements in order to sufficiently reduce the NTP-tagged nanoparticles. Applying the chosen potential to the TRC, reductive transients were observed. From this, the number of NTP molecules was calculated and compared with two theoretical models: a solid sphere, and a completely porous nanoparticle formed by aggregation of a large number of smaller particles. This therefore allows an estimation of the PtNP porosities, which can be further confirmed by the TEM images (Fig. 2(a) and (b)).

Initial experiments were conducted to explore the redox properties of molecular NTP adsorbed on both glassy carbon electrode and PtNP surfaces. First, a glassy carbon electrode was modified by NTP molecules (Supporting Information) before being transferred to an aqueous solution of 10.0 mM  $\text{HClO}_4$  and 30.0 mM  $\text{NaClO}_4$ . CVs were recorded and a reductive peak was obtained at ca.  $-0.4$  V (vs SCE), as shown in Fig. 2(a). In the absence of NTP, no signal was observed (red



**Scheme 1** The four-electron reduction of adsorbed NTP.

line in Fig. 2 (a)), indicating the peak was due to the NTP reduction. This response likely corresponds to a four-electron, four-proton reduction of the nitro group to the hydroxylamine<sup>28–30</sup> (Scheme 1).

Next, a glassy carbon electrode was modified with NTP-tagged PtNPs (Supporting Information) and analogous experiments were performed. A reductive wave was observed at ca.  $-0.2$  V (vs SCE) and again attributed to the reduction of NTP, as shown in Fig. 2(b).<sup>†</sup> No peak was seen when drop casting stock PtNPs (red line in Fig. 2 (b)). The NTP reduction peak potentials varied between glassy carbon to PtNP surfaces, representing the different environments influencing possibly both the thermodynamics and kinetics of the process. Therefore, based on the voltammetric response of NTP adsorbed on PtNPs, an applied potential of  $-0.25$  V (vs SCE) was chosen for the nanoimpact experiments such that measurements were recorded at sufficiently negative potentials in order to maximise the obtained reductive current by ensuring full reduction of the surface layers.

Finally, nanoimpact measurements were conducted to investigate the reductive charge of NTP per nanoparticle. Chronoamperograms (CAs) were recorded in an aqueous

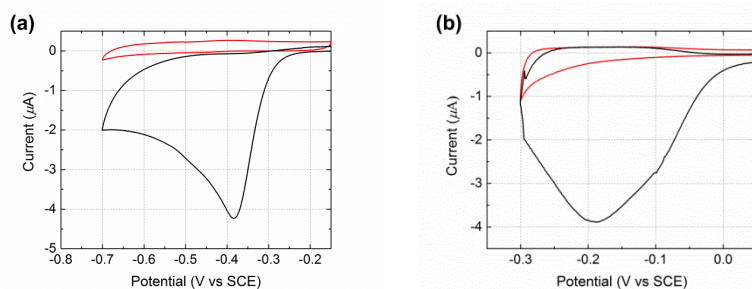


**Fig. 2** CVs for a glassy carbon macroelectrode with (black) or without (red) modification of (a) NTP and (b) NTP-tagged PtNPs. All scans were performed in a nitrogen saturated solution of 10.0 mM  $\text{HClO}_4$  and 30.0 mM  $\text{NaClO}_4$  at a scan rate of  $25 \text{ mV s}^{-1}$ .

electrolyte of 10.0 mM  $\text{HClO}_4$  and 30.0 mM  $\text{NaClO}_4$  at  $-0.25$  V (vs  $\text{Ag}/\text{AgCl}$  (1.0 M  $\text{KCl}$ )). This potential was carefully selected from the drop-casting experiment (Fig. 2(b)) and was sufficient for a complete reduction of the adsorbed NTP. In the experiments, 60 pM NTP-tagged PtNPs were added and spikes were clearly observed with an approximately millisecond duration, as shown in Fig. 3 (black line). These are attributed to the reduction of the nitro group taking place when the NTP-tagged PtNPs make contact with the carbon fibre substrate. No impact spikes were observed in the case of untagged PtNP or electrolyte only, confirming that the reduction of NTP on the surface of the nanoparticles is the source of the transients (red line in Fig. 3(a)).

The average charge passed per transient ( $Q / C$ ) was found to vary with the NTP modification time of the nanoparticles: it increased up to 5 hr and then leveled off as shown in Fig. 4. The reason for this is probably because the tag molecule continually adsorbs onto the PtNP surface until a complete self-assembled monolayer (SAM) forms.<sup>31-32</sup> The surface was saturated after 5 hr and thus no additional NTP can be inserted at a longer modification times ( $t / \text{hr}$ ).

A total of 160 spikes obtained at 5, 10, 20 and 30 hr modification times were analysed, corresponding to impacts of particles with a full NTP monolayer coverage. A mean charge of  $0.094 \times / 1.1$  pC passed per impact transient ( $Q / C$ ) was calculated,<sup>33,6</sup> which is related to the number of tag molecules ( $N_{\text{NTP}} / \text{molecules}$ ) via the electronic charge ( $e / C$ ) according to

$$Q = 4eN_{\text{NTP}} \quad (1)$$

Hence, the average number of NTP attached to the surface of a single PtNP can be calculated as  $(1.5 \times / 1.1) \times 10^5$  molecules, from the experimental measurement of the transients. This can be further discussed and compared with the results from two simple geometric models.

For Model 1, the assumption was made that the PtNP is a solid, smooth sphere of radius 25 nm and its surface area ( $S_{\text{PtNP, solid}} / \text{m}^2$ ) is

$$S_{\text{PtNP, solid}} = 4\pi R^2 \quad (2)$$

where  $R$  is the radius of the non-porous, solid spherical PtNP. Assuming optimal close-packing was adopted by the NTP molecules on a two-dimensional surface plane, the fractional filling efficiency ( $f_1$ ) is 0.91 for spheres or ellipses<sup>34</sup> and the surface area of a PtNP ( $S_{\text{PtNP}} / \text{m}^2$ ) can be written as

$$f_1 \times S_{\text{PtNP}} = A_{\text{NTP}} \times N_{\text{NTP}} \quad (3)$$

where  $A_{\text{NTP}}$  is the adsorption area occupied per NTP, as reported by literature ( $1.1 \times 10^{-19} \text{ m}^2$ ).<sup>35</sup> Combining Equation (2) and (3) gives

$$N_{\text{NTP}} = (4\pi R^2 \times f_1) / A_{\text{NTP}} \quad (4)$$

Therefore, the number of NTP adsorbed per nanoparticle can be determined as  $6.5 \times 10^4$  molecules due to the formation of a SAM, or less when the modification was incomplete.

In Model 2, each PtNP (ca. 25 nm radius) was an aggregate of identical small nanoparticles (ca. 2.5 nm radius, estimated from Fig. 2(b)). As it is difficult to know the inner configuration of the aggregates from the TEM images, these small solid spheres were assumed to arrange in a densest close-packing in space and the fractional filling efficiency ( $f_2$ ) is 0.74.<sup>34</sup> As the volume of a spherical PtNP ( $V_{\text{PtNP}} / \text{m}^3$ ) is

$$V_{\text{PtNP}} = (4\pi/3) R^3 \quad (5)$$

the space occupied by the small nanoparticles is  $f_2 \times V_{\text{PtNP}}$ . This can be written as

$$f_2 \times V_{\text{PtNP}} = (4\pi/3) r^3 \times n \quad (6)$$

where  $r$  is the small nanoparticle radius (ca. 2.5 nm) and  $n$  is the number of small nanoparticles per PtNP. Since

$$r = 0.1 R \quad (7)$$

combining Equations (5), (6) and (7), a number of ca. 740 (1000  $f_2$ ) small nanoparticles were determined to be present in one PtNP. Therefore, the surface area of a porous PtNP ( $S_{\text{PtNP, porous}} / \text{m}^2$ ) is

$$S_{\text{PtNP, porous}} = 1000 f_2 \times 4\pi r^2 \quad (8)$$

Substituting Equation (8) into (3) yields

$$N_{\text{NTP}} = (1000 f_1 f_2 \times 4\pi r^2) / A_{\text{NTP}} \quad (9)$$

The number of tag molecules per PtNP is then  $4.8 \times 10^5$  for full NTP adsorption, or fewer at an insufficient modification time.

Comparing the number of NTP obtained from experiments ( $1.5 \times 10^5$  molecules) with the ones from solid ( $6.5 \times 10^4$  molecules) and porous ( $4.8 \times 10^5$  molecules) PtNP models, the experimental result is between the two extremes and closer to the fully porous case, suggesting a significant degree of porosity in the PtNPs used. TEM images also reveal clusters of small nanoparticles (Fig. 1(a)), but the knowledge of their internal packing was limited. We conclude the NTP molecules can partially insert into the PtNP aggregates, and undergo adsorption at their inner surface.

This result is significant as first it extends the method of TRC

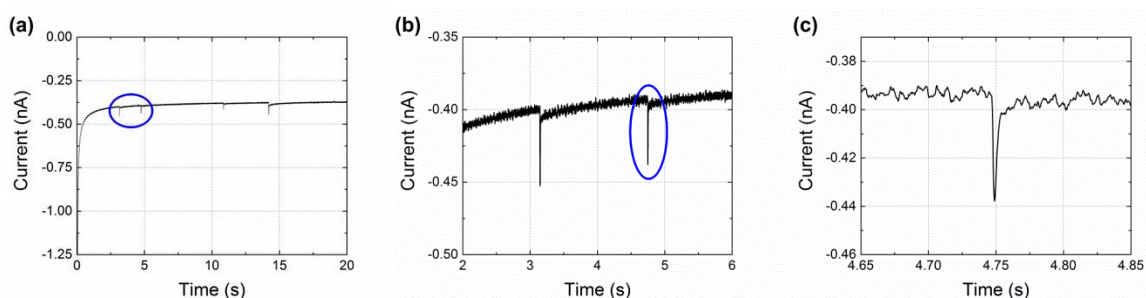


**Fig. 3** (a) Chronoamperometric profiles with NTP-tagged PtNPs. (b) A zoom of circled reductive transients in (a). (c) Further amplification of the circled spike in (b). All scans were recorded in a nitrogen saturated solution of 10.0 mM  $\text{HClO}_4$  and 30.0 mM  $\text{NaClO}_4$  and potentiostatted at  $-0.25$  V vs  $\text{Ag}/\text{AgCl}$  (1.0 M  $\text{KCl}$ ).



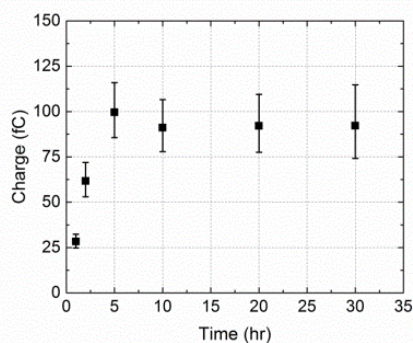


**Fig. 4** The variation of the average charge per impact transient, from overall 251 measurements, as a function of time allowed for NTP molecules to adsorb onto PtNPs.

to investigation of the porosity of nanoparticles. Electrons are transferred via either direct electron transfer or a “hopping” mechanism,<sup>36–37</sup> enabling an in-situ quantification of inner structures for porous nanoparticle. In addition to this, electroactive tag molecules can be suitably selected and reduced or oxidised without destroying the underlying core. Second and most importantly, it can be realised that the electrocatalytic ability and other properties of the nanomaterials cannot be correctly understood without realising their porosities.<sup>8, 16, 38–40</sup> In particular, the extent to which “catalytic” properties can be attributed to a change of effective area or to altered intrinsic activity resulting from either quantum confinement or surface morphology effects, requires a realistic estimation of the “active surface area” of the particle in solution. The assumption that the internal surfaces do not contribute to any (electro-)catalysis may lead to incorrect inferences.

In summary, porous PtNPs formed of an aggregate of many ( $10^2$  -  $10^3$ ) much smaller nanoparticles have been shown to present internal surfaces available for electrocatalytic reaction and hence can be inferred to be accessible to the solution phase in which the particles are suspended. The nano-impacts method provides a methodology for the in situ measurement of the “active surface area” of the nanoparticles which is essential in understanding the origin of any catalytic behaviour shown by the nanoparticles.

## Acknowledgement

The research is sponsored by the funding from the European Research Council under the European Union Seventh Framework Programme (FP/2007-2013) / ERC Grant Agreement No. [320403]. Xue Jiao thanks the China Scholarship Council for supporting her DPhil research.

## Notes and references

‡ A background subtraction was performed to reduce the capacitive contribution to the signal.

§ The transient charges from each modification time were dispersed in a lognormal distribution, with the mean  $\mu$  and the standard error of mean  $\sigma/\sqrt{n}$ , as measurements of the minimum current restricted by the potentiostat. To clarify, the “back-

transformed” values in terms of charge ( $Q/C$ ) can be written in a mathematical expression according to the lognormal law, with the median  $\mu^* = e^\mu$  and the multiplicative standard error of mean  $\sigma^*/\sqrt{n} = e^{\sigma^2/n}$ . Therefore the sign  $\times/$  (times/divide) was employed to denote the error, analogous to the  $\pm$  notation used in a Gaussian distribution.

- 1 K. Taeho and H. Taeghwan, *Nanotechnology*, 2014, **25**, 012001.
- 2 P. R. Bandaru, H. Yamada, R. Narayanan and M. Hoefer, *Materials Science and Engineering: R: Reports*, 2015, **96**, 1–69.
- 3 F. Raimondi, G. G. Scherer, R. Kötz and A. Wokaun, *Angewandte Chemie International Edition*, 2005, **44**, 2190–2209.
- 4 R. Tong, H. D. Hemmati, R. Langer and D. S. Kohane, *Journal of the American Chemical Society*, 2012, **134**, 8848–8855.
- 5 A. Chen and P. Holt-Hindle, *Chemical Reviews*, 2010, **110**, 3767–3804.
- 6 A. Chen, D. J. La Russa and B. Miller, *Langmuir*, 2004, **20**, 9695–9702.
- 7 R. A. Thearle, Z. Sofer, D. Bouša and M. Pumera, *ChemPhysChem*, 2016, **17**, 2096–2099.
- 8 N. C. Bigall, T. Härtling, M. Klose, P. Simon, L. M. Eng and A. Eychmüller, *Nano Letters*, 2008, **8**, 4588–4592.
- 9 P. Mani, R. Srivastava and P. Strasser, *Journal of Power Sources*, 2011, **196**, 666–673.
- 10 H. B. Jung, H. Xu, H. Konishi and E. E. Roden, *Journal of Geochemical Exploration*, 2016, **169**, 80–88.
- 11 Y. Chen, Q. Ma, H. Jia and Y. Wang, *Journal of Materials Science: Materials in Electronics*, 2016, DOI: 10.1007/s10854-016-5102-4, 1–7.
- 12 J. Liu, Z. Wang, A. Sheng, F. Liu, F. Qin and Z. L. Wang, *Environmental Science & Technology*, 2016, **50**, 5606–5613.
- 13 S. V. Sokolov, K. Tschulik, C. Batchelor-McAuley, K. Jurkschat and R. G. Compton, *Analytical Chemistry*, 2015, **87**, 10033–10039.
- 14 B. Ni and X. Wang, *CrystEngComm*, 2015, **17**, 6796–6808.
- 15 J. Snyder, I. McCue, K. Livi and J. Erlebacher, *Journal of the American Chemical Society*, 2012, **134**, 8633–8645.
- 16 H. Guo, X. Liu, C. Bai, Y. Chen, L. Wang, M. Zheng, Q. Dong and D.-L. Peng, *ChemSusChem*, 2015, **8**, 486–494.
- 17 B. Han, C. E. Carlton, A. Kongkanand, R. S. Kukreja, B. R. Theobald, L. Gan, R. O'Malley, P. Strasser, F. T. Wagner and Y. Shao-Horn, *Energy & Environmental Science*, 2015, **8**, 258–266.
- 18 China Pat., 2014.
- 19 E. P. Chang and J. S. Evans, *Biochemistry*, 2015, **54**, 5348–5355.
- 20 Germany Pat., 2015.
- 21 X. Lang, A. Hirata, T. Fujita and M. Chen, *Advanced Energy Materials*, 2014, **4**, 1301809–n/a.
- 22 W. Cheng and R. G. Compton, *TrAC Trends in Analytical Chemistry*, 2014, **58**, 79–89.
- 23 M. Pumera, *ACS Nano*, 2014, **8**, 7555–7558.
- 24 N. V. Rees, *Electrochemistry Communications*, 2014, **43**, 83–86.
- 25 P. H. Robbs and N. V. Rees, *Physical Chemistry Chemical Physics*, 2016, **18**, 24812–24819.
- 26 Y.-G. Zhou, B. Haddou, N. V. Rees and R. G. Compton, *Physical Chemistry Chemical Physics*, 2012, **14**, 14354–14357.
- 27 M. Giovanni, A. Ambrosi, Z. Sofer and M. Pumera, *Electrochemistry Communications*, 2015, **56**, 16–19.
- 28 I. Rubinstein, *Journal of Electroanalytical Chemistry and Interfacial Electrochemistry*, 1985, **183**, 379–386.
- 29 Y.-G. Zhou, N. V. Rees and R. G. Compton, *Chemical Communications*, 2012, **48**, 2510–2512.
- 30 B. J. Plowman, N. P. Young, C. Batchelor-McAuley and R. G.

- Compton, *Angewandte Chemie International Edition*, 2016, **55**, 7002-7005.
- 31 J. U. Nielsen, M. J. Esplandiu and D. M. Kolb, *Langmuir*, 2001, **17**, 3454-3459.
  - 32 F. Cecchet, D. Lis, J. Guthmuller, B. Champagne, Y. Caudano, C. Silien, A. Addin Mani, P. A. Thiry and A. Peremans, *ChemPhysChem*, 2010, **11**, 607-615.
  - 33 E. Limpert, W. A. Stahel and M. Abbt, *BioScience*, 2001, **51**, 341-352.
  - 34 T. Matsumoto and W. Nowacki, in *Zeitschrift für Kristallographie*, 1966, **123**, 401.
  - 35 N. V. Rees, Y.-G. Zhou and R. G. Compton, *Chemical Physics Letters*, 2012, **525-526**, 69-71.
  - 36 C. Amatore, Y. Bouret, E. Maisonhaute, J. I. Goldsmith and H. D. Abruña, *Chemphyschem : a European journal of chemical physics and physical chemistry*, 2001, **2**, 130-134.
  - 37 C. Amatore, Y. Bouret, E. Maisonhaute, J. I. Goldsmith and H. D. Abruña, *Chemistry*, 2001, **7**, 2206-2226.
  - 38 Z. Guo, S. J. Percival and B. Zhang, *Journal of the American Chemical Society*, 2014, **136**, 8879-8882.
  - 39 H. S. Ahn and A. J. Bard, *Angewandte Chemie International Edition*, 2015, **54**, 13753-13757.
  - 40 J. Kim, B.-K. Kim, S. K. Cho and A. J. Bard, *Journal of the American Chemical Society*, 2014, **136**, 8173-8176.